RJC

RASĀYAN *J. Chem.*
Vol. 18 | No. 3 |1606-1619| July-September | 2025
ISSN: 0974-1496 | e-ISSN: 0976-0083 | CODEN: RJCABP
http://www.rasayanjournal.com
http://www.rasayanjournal.co.in

CATALYTIC EFFICIENCY OF NiS/Al_2S_3 NANOPARTICLE WITH VALACYCLOVIR HYDROCHLORIDE BY CHLORAMINE-T IN ACID SOLUTION: DECIPHERING THE KINETICS AND MECHANISM

Sonakshi H. S.[1], Arpitha M.K.[1], Vidyashree K. M.[1] and H. P. Jayadevappa[2,✉]
[1]Chemistry Department, Yuvaraja's College, Mysore 570005 (Karnataka), India
[2]Department of Chemistry, Yuvaraja's College, Mysore, Karnataka, India
✉Corresponding author: hpjayadevappa@gmail.com

ABSTRACT

An electrochemical method was employed to synthesize NiS/Al_2S_3 nanoparticles, with Na_2S serving as the conductive salt, at room temperature and ambient pressure. The synthesized nanoparticle showed an average crystalline size of 5nm with a hexagonal crystal structure. A combination of XRD, SEM, EDX, and FTIR techniques provided insights into the material's size, shape, and chemical composition. The data reveals the adverse catalytic property of the nanoparticle. The synthesized NiS/Al_2S_3 nanoparticle was used as a catalyst to study the degradation of Valacyclovir (VCL) by N-Chloro-p-toluensulfonamide (CAT) in low pH solution at 298K. A detailed analysis of the reaction stoichiometry and oxidation products was performed for both nano-catalyzed and non-nano-catalyzed reactions. The reaction rate's influence on [CAT] is unimolecular, while the proportionality to [VCL] is fractional-order, for both nano-catalyzed and non-nano-catalyzed reactions. The influence of hydrogen ion concentration on reaction kinetics differs between the non-nano-catalyzed and nano-catalyzed reactions, with an inverse proportionality to a fractional power observed for the former and a non-integer order dependence observed for the latter. The reaction rate is not appreciably affected due to the accumulation of the resulting compound. A negligible negative correlation between the permittivity constant and reaction rate was found for both cases. The independence of the reaction rate on ionic strength implies that non-ionic species play a crucial role in the rate-limiting step. No evidence of free radical intermediates was found, and kinetic studies at different temperatures enabled the calculation of thermodynamic parameters. A plausible mechanism was proposed to explain the observed kinetic parameters, and rate laws were formulated for both catalyzed and nano-catalyzed reactions.

Keywords: Kinetics, Valacyclovir, Chloramine-T, Nano-Catalyzed, Mechanism, Stoichiometry.

RASĀYAN *J. Chem.*, Vol. 18, No. 3, 2025

INTRODUCTION

Chloramine-T (CAT), a powerhouse in the organic haloamine family, boasts an impressive chemical profile as N-Chloro-p-toluene sulfonamide, making it a significant entity in the realm of organic chemistry.[1] The pH-invariant oxidation capabilities of CAT enable its effective deployment in various chemical environments, including acidic and basic media. The oxidative profile of organic halo amines closely resembles that of hypohalites, albeit with improved stability, thereby enhancing their potential for various chemical applications. Aromatic sulphonyl halo amines were found to be utilized to investigate the degradation kinetics of diverse molecular compounds. The oxidizing capabilities of CAT are notable for their mildness, stability, and non-toxicity, making it a valuable reagent in various chemical contexts. CAT's antimicrobial properties confer upon its great biological significance, as it serves as a vital component in the fight against microbial diseases.[2-6] CAT, a prominent representative of the organic halo-amine class, participates in a diverse range of reactions with various functional groups, facilitating a wide array of molecular transformations, with its kinetic and mechanistic properties being extensively characterized.[7-10]

Valaciclovir (valacyclovir), L-valine-2-[(2-amino-6-oxo-9-hipurin-9-yl)methoxy]ethyl (2*S*)-2-amino-3-methylbutanoate is an antiviral drug. Valacyclovir [VCL] is also called Valtrex. VCH, a precursor to acyclovir, shows effectiveness against herpes viruses and varicella-zoster virus, making it a promising treatment option. VCL belongs to the class of purine nucleoside analogue drugs. The antiviral properties of VCH have been harnessed for many years to treat and manage herpes infections, including herpes simplex

and herpes zoster, in addition to preventing cytomegalovirus infection in organ transplant patients. VCL was patented in 1987, paving the way for its introduction into medical use in 1995.[11-15] VCL is listed as an essential medicine by the WHO and can be obtained as a generic medication, making it accessible to a broader patient population. Drugs in this class are commonly used in the management of hepatitis, HIV, and cytomegalovirus infections. VCL is commonly prescribed to treat oral and genital herpes outbreaks, providing relief from symptoms and reducing the frequency of recurrences. Genital herpes, a common sexually transmitted infection, affects over 400 million people worldwide due to the herpes simplex virus (HSV). The herpes virus causes a lifelong infection with recurring episodes. VCL is a medication that stops the virus from multiplying by blocking its DNA production, reducing the severity of the infection. Infected cells take up VCL, and a viral enzyme converts it into its active form, allowing it to effectively inhibit viral DNA replication. Acyclovir triphosphate's preferential binding to viral DNA polymerase ensures targeted inhibition of viral replication with minimal impact on host cell DNA synthesis. The bioactive of valacyclovir involves its rapid conversion to acyclovir, which is then phosphorylated to acyclovir triphosphate. Chain termination occurs when acyclovir triphosphate is incorporated into viral DNA, preventing further viral replication. Valacyclovir research encompasses various aspects of the drug, including its chemical structure, analytical methods, biodegradation pathways, and mechanism of action.[16-20] Nanoparticles have revolutionized various manufacturing sectors because of their exceptional properties, including tiny size, increased surface area, as well as impressive absorption capabilities, making them an indispensable tool in modern technology. Enabling smaller, faster, and more powerful data storage and processing systems. Various nanoparticle preparation methods are available, including sol-gel, electrochemical, thermal, and green synthesis. The electrochemical method is a versatile and controllable technique for synthesizing nanoparticles, leveraging the principles of electrochemistry to reduce metal ions in solution to form nanoparticles.[21] To date, no studies have investigated the degradation of valacyclovir using CAT and nanoparticles as catalysts. We present a comprehensive kinetic study of the catalysed and uncatalyzed reactions of valacyclovir by CAT in the presence of NiS/ Al_2S_3 nanoparticles, exploring the underlying mechanistic and thermodynamic aspects in acidic aqueous medium at 298K.

EXPERIMENTAL

NiS/Al_2S_3 Nanoparticles' Synthesis by the Electrochemical Method

In this study, we employed an electrochemical approach to synthesize NiS/Al_2S_3 nanoparticles using nickel and Aluminium electrodes in an aqueous solution containing 0.5% Na_2S as a conductive salt, facilitating the formation of these multifunctional nanoparticles. The electrodes were carefully positioned within a custom-designed holder, facilitating complete submersion in the electrolytic solution. The electrodes were separated by a uniform distance of 1 cm to ensure optimal electrochemical performance. The electrolysis experiment was conducted at room temperature (approximately 25°C) using 50 mL of Na_2S solution, maintained for 5 hours under static conditions (i.e., without stirring). The electrochemical cell was operated under galvanostatic conditions, with the potential being adjusted to achieve a controlled current density of 12 mA. The anodic dissolution of nickel and aluminium electrodes during electrolysis led to the generation of Ni^{2+} and Al^{3+} ions. The electrochemical reaction between these metal ions and sodium sulphide solution resulted in the nucleation and growth of NiS/Al_2S_3 nanoparticles. The variation in redox potentials among Ni^{2+} and Al^{3+} ions gives rise to differences in their electrochemical reactivity, affecting the overall reaction kinetics and nanoparticle formation. Al_2S_3 forms faster than NiS because aluminium has a more negative dissolution potential (-1.662eV) than nickel (-0.28). A multi-step purification protocol was employed to remove impurities from the synthesized nanoparticles, involving repeated aqueous washing, centrifugal separation, and high-temperature calcination (600 °C, 4hours) to eliminate sodium and sulphide residues. The underlying mechanism governing the electrochemical synthesis of NiS/Al_2S_3 nanoparticles is outlined as follows.

Experimental Procedures and Techniques

CAT, a potent oxidizing agent from Sigma, was dissolved in double-distilled water to create an aqueous mixture. The solution was standardized using the iodometric method and stored in a brown bottle to protect it from light degradation. Standardization of the solution by iodometric titration was followed by storage in an amber glass bottle to maintain stability. Before each experiment, an aqueous solution of VCL (Sigma)

was prepared at the desired concentration. A predetermined amount of NiS/Al_2S_3 nanoparticle catalyst was added to the reaction mixture for catalysis. It is synthesized by the electrochemical method in the laboratory, and analysis has been done for confirmation. Reagents of analytical reagent grade were utilized for the experiment, unless alternative grades were specified. The solvent employed for the kinetic investigations was double-distilled water. A potassium nitrate solution was prepared by dissolving the salt in purified water to maintain ionic balance. The dielectric properties of the reaction solution were modulated by adding methanol in varying quantities. The other chemical utilized conformed to analytical grade purity standards. Double-purified water was employed as the solvent for solution preparation to ensure consistent results. Double-purified water was used to prepare solutions, ensuring consistent and reliable results.

Kinetic Profile Determination

To simplify kinetic analysis, experiments were performed under a pseudo-unimolecular-order environment with [VCL] in significant surplus over [CAT]. Calibrated quantities of VCL, hydrochloric acid, and sodium chloride solutions were combined in the tightly sealed borosilicate tube to generate the reaction mixture, which was then subjected to kinetic analysis. A fixed total volume was maintained across all experimental runs by adding the appropriate volume of water. The reaction mixture was maintained under thermostatic conditions at 298K for an adequate period. A measured amount of pre-equilibrated sodium Tosylchloramide sodium solution was subsequently added to the mixture, then subjected to thorough mixing. A specific gram of NiS/Al_2S_3 nanoparticles was incorporated into the reaction mixture as a catalyst. Following pipetting, the mixture was quickly decanted into a laboratory vessel filled with frosty aqueous medium. The reaction's kinetic parameters were determined by monitoring the unreacted [CAT] in two milliliter subsets of the reaction solution using iodometric analysis at a set of time intervals. A high level of reproducibility (±3%) variation was noticed in the pseudo-unimolecular order kinetic constant, obtained from log-linear plots of chloramine-T concentration as a function of time. The velocity of the reactions was identified by drawing tangents to the curve at specified concentrations of CAT and NiS/Al_2S_3, and calculating the corresponding slopes. By analyzing a log-log plot of reaction kinetics (-dc/dt) vs. substrate concentration, the kinetic behavior of the reaction was elucidated, and the kinetic order of reaction for each reactant was determined.

Stoichiometry Analysis as well as Product Identification of Reaction

Thermodynamic equilibrium was achieved for a set of reaction solutions containing VCL, NiS/Al_2S_3 nanoparticles, and excess CAT after 48 hours at 298K. Excess CAT was used in the kinetic experiments, and the amount of unreacted CAT present at the end of the reaction confirmed a 1:2 CAT-to-VCL stoichiometry. As a result, the stoichiometric equation was determined to be:

$$C_{13}H_{20}N_6O_4 + 2\ PTSO_2NClNa + H_2O \xrightarrow{NiS/\ Al_2S_3} C_7H_{13}NO_3 + C_6N_4H_7O_2 + 2PTSO_2NH_2 + 2Na^+ + 2Cl^-$$

Where $PT = CH_3C_6H_4$

The predominant product of the reaction was determined as 2-amino-1,4,5,9-tetrahydro-6H-purin-6-one and 2(carboxyoxy) ethyl valinate. Following evaluation, the most effective solvent for product extraction was found to be 1,1'-Oxybisethane. Following treatment with aqueous sodium hydroxide solution, the ether layer was subjected to a spot test[22] to identify the degradation compound of the disubstituted amine and carboxylic acid chemical substrate. The compound was treated with nitrous acid, and the resulting test indicated the existence of a dialkyamino-hydrocarbon moiety. PTS, the hydrogenation product of chloramine-T, was isolated in acetoxy ethane and characterized by TLC with ethoxyethane-based mobile phase, trichloromethane, and butyl hydroxide (2:2:1) and I_2 as the detecting reagent, resulting in an Rf value of 0.839.

RESULTS AND DISCUSSION

XRCD X-Ray Crystallography Diffraction

Composition was confirmed by XRCD examination and crystalline structure from the synthesized nano-powder. Two sharp reflection signals are recorded at 2θ angles 38.2 and 50.5, which were indexed as (110) and (211), respectively. The observed peaks match with standard JCPDS pattern No. 03-065-3419, confirming the presence of hexagonal NiS in the sample. The 2θ values of 25° and 52.71° were assigned to the (104) and (208) Miller indices. The existence of Al_2S_3 in the analyte was verified by four distinct signals, which match the standard JCPDS pattern No. 01-084-2321. A thorough examination of the Crystalline

domain size is carried out using the W-H chat technique, with the results graphically represented in Fig.-1(b). The Willium-hall technique enables a maths analysis of XRD signals broadening, resulting in microstrain and crystallite size effects. Employing the Willum-Hall technique, from the UDM scattered plot featuring 4sinθ and βcos θ, a crystallite size of 0.1355 μm was calculated using linear fits' y-intercept and slope values. The size of the crystallites was found to be approximately 5.02nm.

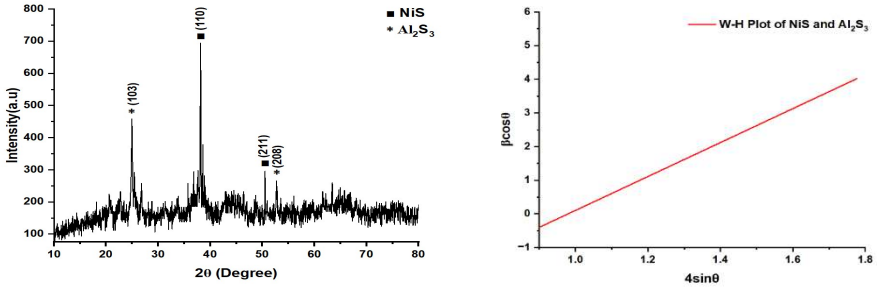

(a) (b)

Fig.-1: XRD Pattern of a) Nanoparticle-NiS/Al_2S_3 and b) W-H Plot Analysis

Investigation of NiS/Al_2S_3 Nanoparticle Structure and Composition by FE-SEM and EDS

Scanning electron microscopy (SEM) analysis (Fig.-2) demonstrated that the catalytic activities of electrochemically synthesized nanoparticles are largely governed by their particle size and surface area. SEM analysis revealed that the sample consisted of agglomerated particles, and EDAX was used to examine the elemental composition of the NiS/Al_2S_3 nanoparticles. EDAX analysis confirms the elemental composition of the NiS/Al_2S_3 nanoparticle, as shown in the spectrum (Fig.-3). The graph shows distinct peaks corresponding to NiS/A_2lS_3, indicating their presence in the prepared sample. The quantitative outcome from FE-SEM EDS examination, indicating the elemental composition, along with their relative proportions, is summarized in the accompanying data.

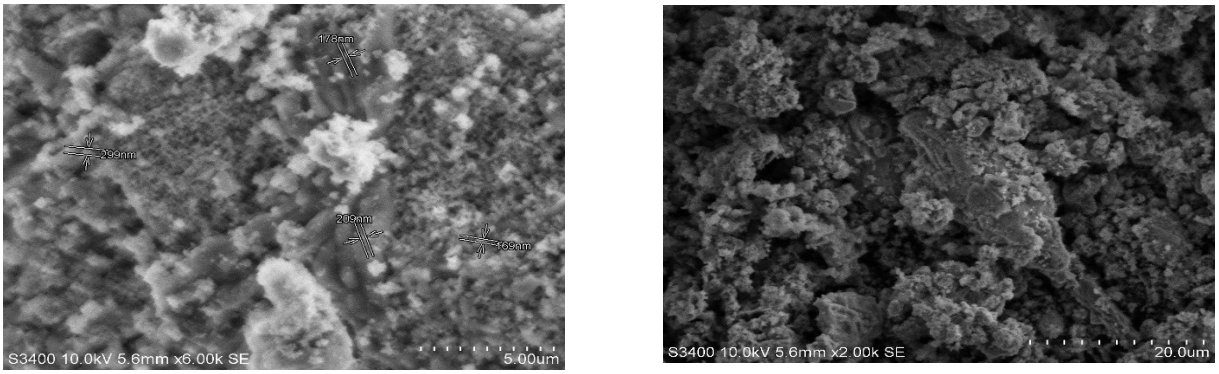

Fig.-2: SEM image of Electrochemically Synthesized NiS/Al_2S_3 Nanoparticle

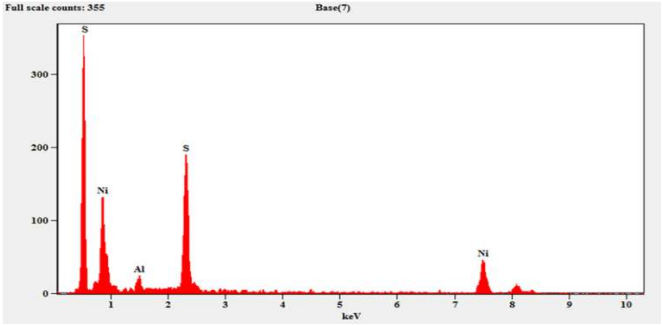

Fig.-3: X-ray Analysis of EDS of the Electrochemically Synthesized NiS/Al_2S_3 Nanoparticle

Table-1: Summary Statistics

Table-1: Summary Statistics

Element Line	Weight %	Weight % Error	Atom %
Al K	2.12	± 0.20	1.78
S K	70.59	± 1.76	87.68
S L	---	---	---
Ni K	27.30	± 2.42	10.54
Ni L	---	---	---
Total	100.00		100.00

Fourier Transform Infrared Spectroscopy

To confirm the successful reduction and dispersion of chemical components, Fourier transform Infrared spectra facilitated the investigation of biological molecule-composite interactions in the fabrication of Al_2S_3 and NiS nanocomposites. As depicted in the figure, the strong absorption signals at 614.68 and 629.51 cm^{-1} are attributed to the O-H stretching vibration in the amide group. 1075.15, 2029.47, and 2209.99 cm^{-1} are peaks obtained from the graph in the Fig.-4.

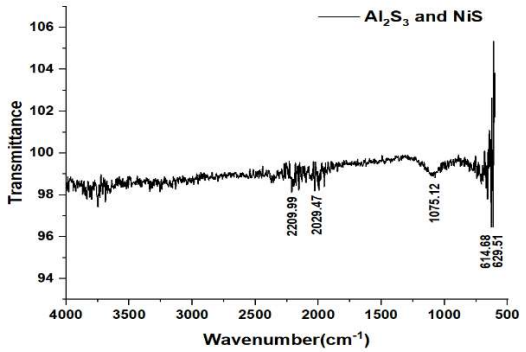

Fig.-4: FTIR Patterns of Al_2S_3/ NiS Nanoparticle

Impact of Variation of the [Chloramine-T] on the Reaction Rate

$$k_1 = \frac{-(dc/dt)}{[\mathrm{CAT}]}$$

Kinetic studies were conducted by pseudo-unimolecular-order reaction kinetics. In contrast, the concentration of VCL is significantly higher than that of the catalyst ([VCL>>[CAT]). The oxidation of VCL was evaluated with and without Al_2S_3/NiS nano-particles, with variations in catalyst concentration ([CAT]) while maintaining constant [VCL], acid, nanoparticle, and temperature conditions. In the beginning, reaction rates were quantitatively determined and systematically recorded for all kinetic reaction trails. A tangent line was drawn to the kinetic reaction curve at the exact point, corresponding to a particular [Chloramine-T], to determine the initial reaction rate. By drawing a tangent to the kinetic reaction curve, the beginning reaction velocity can be determined from its slope. The curve was analyzed by drawing a tangent at a fixed time point. A quantitative evaluation of the tangent slope enabled the determination of the pseudo-unimolecular-order rate constant (k^I). For both nano-catalyzed and non-nano-catalyzed reaction's constant k^I values with the variation of [oxidant] demonstrated that the rate is 1st order with respect initial concentration of Chloramine-T.

Impact of [Valacyclovir] Concentration on Kinetics Process

The behavior under varying conditions of $[VCL]_0$ concentration in the context of the reaction process was examined under identical experimental conditions. The k′ values showed a rising trend with increasing [VCL] concentrations (Table-2). Fig.-5 shows a linear relationship between log k′ and log $[VCL]_0$, indicating a fractional order dependence with a slope of 0.53383 with R^2=0.9728 value and 0.4108 with R^2=0.9346 value for both nano-catalyzed and non-nano-catalyzed processes, respectively.

Impact of Acidic Conditions on Reaction Rate

From the Fig.-6 shows that on changing the concentration of $[H^+]$ from 10 $mmolL^{-1}$- 90$mmolL^{-1}$ follows inverse non-integer order of the molecular reactions in the absence of nano-catalyzed reaction rate in

contrast, kinetics of reaction shows the non-integer reaction order rates in the presence of NiS/Al_2S_3 nano-particles, while maintaining other variables constant. Log k^I vs log$[H^+]$ plots show linear relationships with slopes 0.48 (negative) with R^2=0.981 value and 0.42 (positive) with R^2=0.9993 value for non-nano-catalyzed and nano-catalyzed reactions, respectively.

Table-2: Influence on [VCL], [Chloramine-T], [Hydrogen ion], [Chloride ion], then NiS/Al_2S_3 on the Degradation of the Valacyclovir by Chloramine-T, Without-Nano-Catalyst, With Nano-Catalyst in the Acid Solution at 298K

10^4×[VCL] ($molL^{-1}$)	10^5×[CAT] ($molL^{-1}$)	10^3×[HCl] ($molL^{-1}$)	10^3×NiS/Al_2S_3 (gm)	ku (s^{-1})	kc (s^{-1})
3	5	5	8	5.67	10.87
5	5	5	8	6.39	13.05
7	5	5	8	7.66	17.06
9	5	5	8	9.07	19.21
3	3	5	8	5.58	10.82
3	5	5	8	5.64	10.87
3	7	5	8	5.60	10.91
3	9	5	8	5.37	10.84
3	11	5	8	5.55	10.93
3	5	1	8	12.99	7.19
3	5	3	8	8.18	9.85
3	5	5	8	5.67	10.87
3	5	7	8	4.42	15.77
3	5	9	8	3.98	19.19
3	5	5	4	-	10.78
3	5	5	6	-	10.77
3	5	5	8	-	10.87
3	5	5	10	-	10.92
3	5	5	12	-	10.69

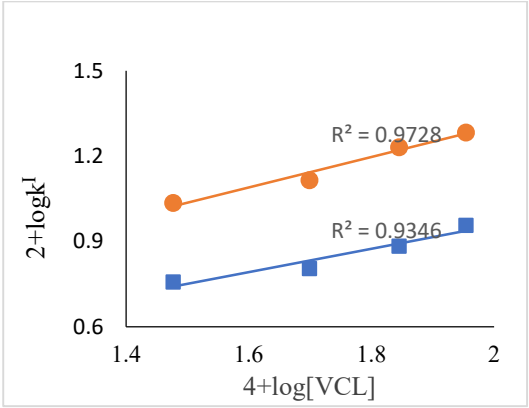

(a)4+log [VCL] nanoparticle catalyzed (b) 4+log [VCL] uncatalyzed

Fig.-5: Impact of [VCL] on Reaction rate at 298K. [VCL] = 3×10^{-4} mol/L, $[NiS/Al_2S_3] = 8\times10^{-3}$g

Relationship Between Ionic Strength and Reaction Kinetics

An investigation was conducted to examine the impact of ionic activity on the reaction kinetics of nanoparticle-catalyzed and nanoparticle-catalyzed reactions. The ionic activity was modulated by adjusting the $[NaClO_4]$ between 0.1 and 1 $molL^{-1}$, meanwhile retaining all other parameters constant. The experiment shows there is no appreciable variation occurring in the rate. It applies to both nano-catalyzed and nano-catalyzed kinetic processes. The unchanged reaction rate indicates that non-ionic species control the key step in both cases.

Investigating the Variation in Electric Permittivity of Chemical Reaction Kinetics

A study of the reaction rate was conducted in media with varying dielectric permittivity (D), with each parameter held constant, to determine the effect of dielectric permittivity.

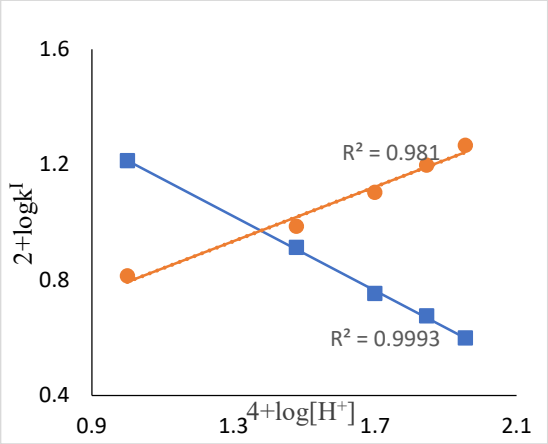

(a) 4+log [Hydrogen ion] with nano-catalyst (b) 4+log [Hydrogen ion] without nano-catalyst

Fig.-6: Impact on $[H^+]$ of Kinetics of reaction at 298K.

$[Chloramine\text{-}T] = 4\times10^{-5}$ $molL^{-1}$ $[NiS/Al_2S_3] = 8\times10^{-3}$gm

The relationship between the rate constant and the dielectric permittivity of the medium is given by:

$$\log k_1 = \log k_o - \frac{z_A z_B e^2 N}{2.303(4\pi€)d_{AB}RT} \times \frac{1}{D}$$

The parameters in the equation are defined as follows: Z_A and Z_B, charges of the reacting ions; k_o, rate constant at infinite dielectric constant; transition state complex size; T, Temperature; and D, medium electric activity. The work of Frost and Pearson has explored the varying effects of solvent composition on reaction kinetics. The dielectric property of the medium's environment was studied using methyl alcohol as a solvent for both non-nano-catalyzed and nano-catalyzed reactions. Table-3 reveals that the reaction rate decreases with increasing dielectric permittivity for the set of two reactions without nano-catalyzed and with nanoparticle-catalyzed processes. To investigate the variation of electric permittivity on chemical reaction kinetics, methanol was added to the reaction medium in varied proportions (0-40%, volume/volume). Fig.-7 illustrates a downward trend line between log k^I and 1/D, and the reciprocal of the dielectric constant (1/D). Separate blank experiments verified that methanol ionization remained below 1% under the experimental conditions.

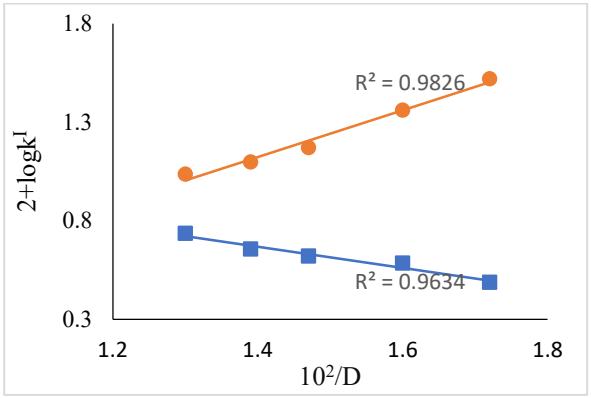

(a) [MeOH] with nano-catalyst (b) [MeOH] without nano-catalyst

Fig.-7: Variation of Dielectric Permittivity on Kinetics

Table-3: Kinect Changes with Variation of Dielectric Permittivity

CH_3OH %vol/vol	D	$10^2/D$	ku^I 10^4 s^{-I}	kc^I 10^4 s^{-I}
0	76.7	1.30	5.67	10.87
10	72.4	1.39	4.53	11.08
20	67.4	1.47	4.16	16.99
30	62.7	1.60	3.83	18.55
40	58.1	1.72	3.07	21.o2

$[CAT]= 5\times10^{-5}$ mol/L, $[NiS/Al_2S_3] =8\times10^{-3}$ gm, $[VCL]= 3\times10^{-4}$ $molL^{-1}$, $[H^+] = 5\times10^{-3}$ $molL^{-1}$, T=298K.

Table-3: Kinetics variation with Variation of Dielectric Permittivity

CH_3OH %vol/vol	D	$10^2/D$	$ku^I\ 10^4\ s^{-I}$	$kc^I\ 10^4\ s^{-I}$
0	76.7	1.30	5.67	10.87
10	72.4	1.39	4.53	11.08
20	67.4	1.47	4.16	16.99
30	62.7	1.60	3.83	18.55
40	58.1	1.72	3.07	21.o2

[CAT]= 5×10^{-5} mol/L, [NiS/Al_2S_3] =8×10^{-3} gm, [VCL]= 3×10^{-4} $molL^{-1}$, [H^+] = 5×10^{-3} $molL^{-1}$, T=298K

Influence of the Product Para-Toluene Sulfonamide Concentration on the Rate

Studies with Para-toluene sulfonamide (PTS) as an oxidation revealed that its concentration (1×10^{-4}-10×10^{-4}mol dm^{-3}) has no notable effect on the kinetics of reaction, suggesting neither reaction involves its participation in the pre-equilibrium step for both without nano-catalyzed and with nano-catalyzed chemical reactions.

Thermal Effects on Chemical Process Dynamics

To investigate the effect of temperature on rates, a temperature range of 293-313K was used to study the kinetics of both nano-catalyzed and non-nano-catalyzed reactions. A thorough analysis of the data presented in Table-4 indicates that the rate constant exhibits a consistent increase with thermal level for both nano-catalyzed and non-nano-catalyzed reactions. The linear Arrhenius plot depicted in Fig.-8 indicates, temperature experts a profound influence on reaction kinetics, with the plot serving as a visual representation of this relationship. A thorough kinetic and thermodynamic analysis of the reaction was performed by assessing Ea variables with and without the nanoparticle.

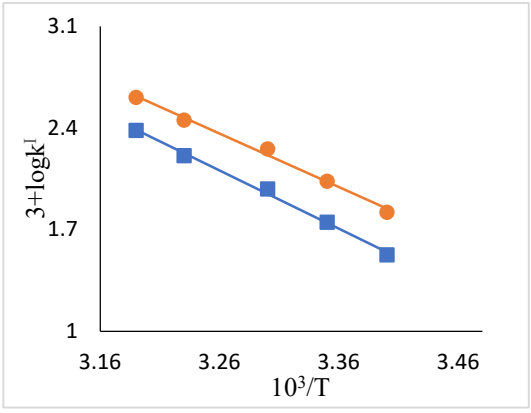

(a) with nano-catalyst (b) without nano-catalyst

Fig.-8 : Variation of Temperature on kinetic of Chemical Reaction: A Comparison of Non-Nano-Catalyzed and Nano-Catalyzed Systems

Table-4: Variation of Temperature on Kinetics of Chemical Reaction on Degradation of VCL by CAT in Acid Solution Along with Activation Variables on Rates

Temperature (K)	ku 10^4 (S^{-I})	kc 10^4 (S^{-I})
293	3.38	6.64
298	5.67	10.87
303	9.58	18.11
308	16.39	28.64
313	24.28	40.99

[CAT]=5×10^{-4} mol dm^{-3}, [NiS/Al_2S_3] = 8×10^{-3} g, [VCL]= 3×10^{-3} mol dm^{-3}, [H^+] = 5×10^{-3} mol dm^{-3}

Reaction Mechanism Without a Catalyst

The oxidation of Valacyclovir by CAT in the medium of water proceeded at a sluggish pace in the absence of nano catalysts. The reaction involves each mole of VCL consuming two moles of CAT.

Table-5: Thermodynamics Profile of Non-Nano Catalyzed and Nano-Catalyzed Reactions

Activation variables	non-nano-catalyzed	nano-catalyzed
E_a (kJ mol^{-1})	83.19	70.36
$\Delta S^{\neq}$ (JK^{-1} mol^{-1})	-1.51	-35.51
$\Delta H^{\neq}$(kJ mol^{-1})	80.71	67.93
$\Delta G^{\neq}$ (kJ mol)	79.98	57.53

The stoichiometric ratio of VCL to CAT in the reaction is 1:2. A rate analysis of the chemical reaction revealed a unimolecular order dependence on the catalyst [CAT], whereas a non-integer order dependence on the concentrations of [VCL] and hydrogen ion concentration. Chloramine-T displays low oxidizing potential in acid and base mixtures, leading to the reduction of substrates with a transfer of two electrons. In aqueous solution, it completely dissociates into ions, behaving as a strong ionizer. In acidic water, it undergoes several equilibria, producing a range of ionic species.[23-25]

$$PTSO_2NClNa \rightleftharpoons PTSO_2NCl^- + Na^+ \quad (2)$$

$$PTSO_2NCl^- + H^+ \rightleftharpoons PTSO_2NHCl \quad (3)$$

$$2\ PTSO_2NHCl \rightleftharpoons PTSO_2NH_2 + PTSO_2NCl_2 \quad (4)$$

$$PTSO_2NCl_2 + H_2O \rightleftharpoons PTSO_2NHCl + HOCl \quad (5)$$

$$PTSO_2NHCl + H_2O \rightleftharpoons PTSO_2NH_2 + HOCl \quad (6)$$

Where PT = $CH_3C_6H_4$.

Consequently, $PTSO_2NHCl$, $PTSO_2NCl_2$, and hypochlorous acid were recognized as excellent oxidizers formed from chloramine-T in acidic aqueous solutions. As the kinetics don't show a 2nd-order relationship with $[CAT]_0$, contrary to equation (4). $PTSO_2NCl_2$ is excluded as a potential reactive species. Additionally, the kinetics of the reaction is not influenced by the presence of N-Chloro-4-methylbenzenesulfonamide, indicating that HCl is not a primary participant in the oxidation process. Consequently, $PTSO_2NHCl$ is deemed as a reactive oxidant moiety. In environments characterized by low pH values (like less than 2 pH), it protonates to form $PTSO_2NH_2Cl^+$.[26,27.]

$$PTSO_2NHCl + H^+ \rightleftharpoons PTSO2NH2Cl^+ \quad (7)$$

The value of the acid dissociation constant in equation (7) at standard temperature 1.02×10^2. The introduction of hydrogen ions inhibits the reaction kinetics, suggesting that proton abstraction of $PTSO_2NH_2Cl^+$ produces the active oxidant moity PTSO2NHCl. A mechanistic scheme (Schematic pathway-1) was represented as rationalizing experimental findings regarding the degradation of VCL from chloramine-T. Here, PTSO2NHCl denotes the active oxidizing species, VCL represents the reactant entity, Xa and Xa^I signify the transition state complex, the transition state complex entity formed during the reaction course. The reaction is initiated by the formation of $PTSO_2NHCl$, which then reacts with the substrate to form an intermediate complex, Xa. This complex consequently undergoes the slowest elementary step in the reaction mechanism, yielding the Xa^I cation complex, eliminating $PTSO_2NH_2$. Intermediate Xa^I undergoes hydrolysis to form Xa^{II}, followed by a reaction with $PTSO_2NHCl$ to generate the products, as illustrated in Schematic pathway-2.

$$PTSO_2NHCl + H^+ \underset{k_2}{\overset{k_1}{\rightleftharpoons}} PTSO_2NH_2Cl^+ \quad \text{(i) speedy reaction step}$$

$$PTSO_2NH_2Cl^+ + VCL \underset{k_3}{\overset{k_2}{\rightleftharpoons}} Xa \quad \text{(ii)speedy reaction step}$$

$$Xa \underset{k_4}{\overset{k_3}{\rightleftharpoons}} Xa^I \quad \text{(iii) rate-determining step}$$

$$Xa^I + H_2O \rightleftharpoons Products \quad \text{(iv) speedy reaction step}$$

The rate equation can be expressed differentially as follows:

$$\frac{d[CAT]}{dt} = k_3[Xa] \quad (8)$$

Let's assume $[CAT]_t$ denote the overall active concentration of the chloramine-T, then:

$$[CAT]_t = [PTSO_2NH_2Cl^+] + [PTSO_2NHCl] + [Xa] \quad (9)$$

$$[CAT]_t = \frac{[PTSO_2NHCl][H^+]}{k_1} + \frac{[Xa]}{k_2[VCL]} + [xa] \quad (10)$$

On solving for Xa,

$$[Xa] = \frac{k_1k_2[CAT][VCL]}{[H^+]+k_1(1+k_2)[VCL]} \quad (11)$$

$$\frac{d[CAT]}{dt} = \frac{k_1k_2k_3[CAT][VCL]}{[H^+]+k_1(1+k_2)[VCL]} \quad (12)$$

The experimentally observed dependencies of the kinetics of reaction on $[VCL]_0$, $[CAT]_0$, and also on the concentration of H^+ are successfully predicted by the rate law (12), which exhibits first-order, non-integer order, and inverse fractional-order kinetics, respectively. Rearranging equation (12), we obtain rate = $k^I[CAT]_0$, which can be further expressed as:

$$k^I = \frac{k_1k_2k_3[VCL]}{[H^+]+k_1(1+k_2)[VCL]} \quad (13a)$$

$$\frac{1}{k^I} = \frac{1}{k_2k_3[VCL]}\left\{\frac{[H^+]}{k_1}+1\right\} + \frac{1}{k_3[VCL]} \quad (14a)$$

A linear regression analysis was performed on the data, utilizing (13a) [th], (14a)[th] to generate graphs k^{I-1} vs $[VCL]^{-1}$ and k^{I-1} vs $[H^+]^{-1}$, thereby facilitating the calculation of k1, k2, and k3. The medium's dielectric permittivity was modified by incorporating different concentrations of 1-methanol (0-40%). The negative permittivity effect observed in the logarithm k^I vs D^{-1} graph implies that dipole-dipole interactions play a substantial role in facilitating the reaction. The introduction of PTS did not result in a discernible change in the reaction rate; these results indicate that the reduction product is not a kinetically competent intermediate in the pre-equilibrium mechanism. The logarithmic plots of k^I against the reciprocal of the dielectric constant (1/D) display a negative slope, indicative of a significant dipole-dipole synchronize component in the reaction mechanism. The insensitivity of the chemical reaction kinetics to changes in ionic strength implies that non-ionic species play a pivotal role in governing the slow-step reaction kinetics.[28-30] Chemical reactions are slightly inhibited by increasing halide ion concentrations. Thermodynamic analysis lends support to the validity of the proposed mechanism. The observed thermodynamic parameters are indicative of a transition state characterized by a high degree of organization and reduced degrees of freedom, suggestive of a tightly bound, compact complex.

Mechanism

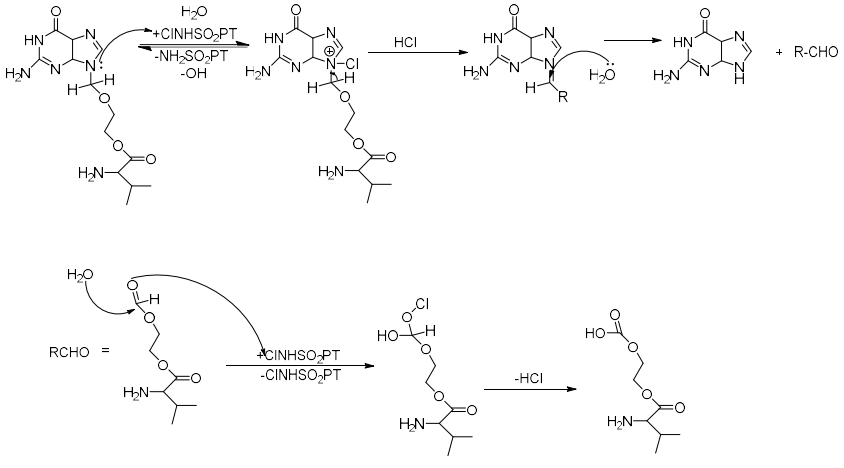

Reaction Mechanism with NiS/Al_2S_3 Nanoparticle Catalyst

A comparative kinetic study of the NiS/Al_2S_3 nanoparticle-catalyzed and non-nanoparticle-catalyzed oxidation of valacyclovir by CAT in aqueous acid solution reveals analogous stoichiometric profiles. Kinetic analysis shows that the reaction rate is directly proportional to the concentration of chloramine-T, indicating 1st order kinetics. On chloramine-T concentration, the reaction kinetics is 1st order, whereas as non-integer order on [NiS/Al_2S_3] nanoparticle. Acidity boosts the reaction kinetics, which depends fractionally on Hydrogen ion concentration. A positive relationship between dielectric permittivity and reaction kinetics is seen, with a slight rise in rate. The entropy changes for the reaction in negative. Evidence suggests that the complexation of the VCL, Chloramine-T, and the NiS/Al_2S_3 nanoparticle in the equilibrium stage is responsible for the observed fractional order dependence on [VCL], highlighting its importance in the reaction pathway.

$$PTSO_2NH_2Cl + H^+ \rightleftharpoons PTSO_2NH_2Cl^+ \quad (15)$$

The addition of H^+ ions leads to a decrease in reaction rate, likely due to the protonation of $PTSO_2NH_2Cl$, forming the protonated species $PTSO_2NH_2Cl^+$. Based on a thorough examination of the experimental data, a plausible rearrangement of the reaction for the NiS/Al_2S_3 nano-catalysed degradation of VCL by chloramine-T is proposed, as depicted in Schematic pathway 3. In this reaction, $PTSO_2NH_2Cl$ serves as the active oxidizing agent, while VCL is the substrate. Before the rate-determining step, NiS/Al_2S_3 interacts with chloramine-T to generate a starting intermediate complex, denoted as Xa^{II}. In the slow kinetic identification stage, VCL reacts with the previously formed transition molecule to produce intermediate Xa^{III} and the $PTSO_2NH_2$ complex, concurrently regenerating the NiS/Al_2S_3 nanoparticle catalyst. As depicted in Schematic pathway-4, the final step of the reaction involves the hydrolytic cleavage of the complex, thereby releasing the desired products.

$$PTSO_2NH_2Cl + H^+ \overset{k_5}{\rightleftharpoons} PTSO_2NH_2Cl^+ \quad \text{(i) rapid equilibrium step}$$

$$PTSO_2NH_2Cl^+ + NiS/Al_2S_3 \overset{k_6}{\rightleftharpoons} Xa^{II} \quad \text{(ii)rapid equilibrium step}$$

$$Xa^{II} + VCL \overset{k_7}{\rightleftharpoons} Xa^{III} + PTSO_2NH_2 \quad \text{(iii) sluggish kinetic step}$$

$$Xa^{III} + H_2O \overset{k_8}{\rightleftharpoons} \text{Products} \quad \text{(iv)rapid}$$

Schematic pathwaye-3

$$PTSO_2NH_2Cl + H^+ \overset{k_5}{\rightleftharpoons} PTSO_2NH_2Cl^+$$

$$PTSO_2NH_2Cl^+ + NiS/Al_2S_3 \overset{k_6}{\rightleftharpoons} PTSO_2NH_2Cl^+ \text{----- } NiS/Al_2S_3$$

The differential rate equation is $\frac{d[CAT]}{dt} = k_7[Xa^{II}]$ (16)

The symbol $[CAT]_t$ denotes the overall amount of CAT, exhibiting high reactivity,

$[CAT]_t = [PTSO_2NHCl] + [PTSO_2NH_2Cl^+] + [Xa^{II}]$ (17)

$k_5 = \frac{[PTSO_2NH_2Cl^+]}{[PTSO_2NHCl][H^+]}$ (18)

$PTSO_2NHCl = \frac{[PTSO_2NH_2Cl^+]}{k_5[H^+]}$ (19)

$k_6 = \frac{Xa^{II}}{[PTSO_2NH_2Cl^+][NiS/Al_2S_3]}$ (20)

$PTSO_2NH_2Cl^+ = \frac{Xa^{II}}{k_6[NiS/Al_2S_3]}$ (21)

$$PTSO_2NH_2Cl^+ = \frac{Xa^{II}}{k_5k_6[NiS/Al_2S_3][H^+]} \quad (22)$$

$$[CAT]_t = \frac{Xaa^{II}}{k_5k_6[NiS/Al_2S_3][H^+]} + \frac{X^{II}}{k_6[NiS/Al_2S_3]} + Xa^{II} \quad (23)$$

$$Xa^{II} = \frac{k_5k_6[NiS/Al_2S_3][H^+]\ [CAT]_t}{1+k_5k_6[H^+]+ k_5k_6[NiS/Al_2S_3][H^+]} \quad (24)$$

Since rate $=k_7[Xa^{III}]$

$$\text{Rate} = \frac{k_5k_6k_7[NiS/Al_2S_3][H^+]\ [CAT]_t}{1+k_5[H^+]+ k_5k_6[NiS/Al_2S_3][H^+]} \quad (25a)$$

The deducted rate law was found to be in excellent agreement with the experimental results, confirming the reliability of the proposed rate model.

$$\text{Reaction rate} = \frac{k_5k_6k_7[NiS/Al_2S_3][H^+]}{1+k_5[H^+]+ k_5k_6[NiS/Al_2S_3][H^+]}$$

On rearranging equation (25), we get

$$\frac{1}{k_c} = \frac{1}{k_7}\{\frac{1}{k_6\,[NiS/Al_2S_3]}(\frac{1}{k_5[H^+]} + 1) + 1\} \quad (26a)$$

Equations (25a) and (26a) indicate that a rectilinear plot of k^{-1} vs. $[VCL]^{-1}$ and inverse concentration of hydrogen ion enables the determination of k_2, k_6, and K_7 from slope and intercepts. The dielectric permittivity of the medium was deliberately altered by incorporating methyl alcohol in concentrations ranging from 0 to 40% (volume/volume). The log k^I vs. 1/D plot showed a negative dielectric effect, indicating dipole interactions. The insensitivity of the reaction rate to the addition of PTS suggests that it is not involved in the pre-reaction equilibrium stage. A negative dielectric effect was seen in the k^I vs. D^{-1} plot, suggesting dipole interactions.[28-30] The kinetics of the reaction did not depend on ionic strength, suggesting a neutral, slow kinetics identification stage. Additionally, the presence of halide ions was found to have a minor inhibitory effect on the reaction kinetics. The thermodynamic variables matched the suggested mechanism. The results suggest that the state of transition adopts a compact, ordered geometry with limited degrees of freedom, which is reflected in the negative entropy of activation and slight positive data for free energy and activation enthalpy.

Mechanism

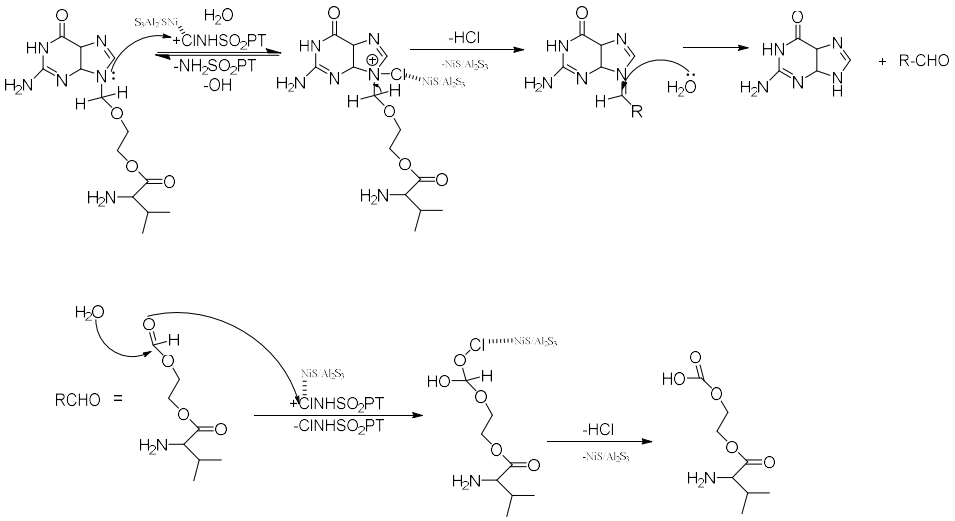

CONCLUSION

The cross-comparison analysis comparative study of degradation of Valacyclovir by CAT in both NiS/Al_2S_3 nanoparticle-catalyzed and without nanoparticle-catalyzed reactions is investigated. The catalytic potency of NiS/Al_2S_3 nanoparticle for the degradation of Valacyclovir by CAT in a water-based acidic environment was studied by comparing with the uncatalyzed reactions. The CAT-VCL redox reaction has been examined in a water-based acidic environment. The degradation of VCL by CAT exhibits a 1:2 stoichiometry,

regardless of whether nanoparticles are present to catalyze the reaction (equation 1). The resulting degradation products were identified as 2-amino-1,4,5,9-tetrahydro-6H-purin-6-one and 2(carboxyoxy) ethyl valinate. Studies were conducted to examine the impact of halide ions and dielectric permittivity on the kinetics of the reaction. The Arrhenius analysis was employed to determine activation variables like energy of activation, degree of freedom, free energy, and enthalpy from the experimentally observed rate constants, providing insight into the reaction mechanism, and the rate law was derived. The results of this study suggest that NiS/Al_2S_3 nanoparticles, prepared through electrochemical synthesis, possess catalytic properties that enhance the degradation of valacyclovir by chloramine-T, highlighting their potential applications in environmental remediation.

ACKNOWLEDGEMENTS

We acknowledge with gratitude the support from the Mysore University, Mysuru, for providing access to instrumental and lab resources in our Chemistry department, Yuvaraja's College, facilitating the kinetic study. The authors wish a warm thanks to the reviewers for greatly improving our research paper.

CONFLICT OF INTEREST

No potential conflict of interest was reported by all authors.

AUTHOR CONTRIBUTIONS

The present work is related to *SDG-3: Good health and Well-being*. All the authors contributed significantly to this manuscript, participated in reviewing/editing and approved the final draft for publication. The research profile of the authors can be verified from their ORCID ids, given below:

Sonakshi H.S. https://orcid.org/0009-0007-1500-0758
Arpitha M.K. https://orcid.org/0009-0007-4983-1701
Vidyashree K.M. https://orcid.org/0009-0009-8151-8015
Jayadevappa H. P. https://orcid.org/0000-0003-4925-7782

REFERENCES

1. S. Malke, S. Shidhaye and V.J. Kadam, *Indian Journal of Pharmaceutical Science*, **69**, 211(2007), https://doi.org/10.4103/0250-474X.33145
2. E. Kolvari, A. Ghorbani-Choghamarani, P. Salehi, F. Shirini and M.A. Zolfigol, *Journal of the Iranian Chemical Society*, **4**, 126(2007), https://doi.org/10.1007/BF03245963
3. A. Sukhdev, A.S. Manjunatha and P. Puttaswamy, *International Scholarly Research Notices*, **1**, (2013), https://doi.org/10.1155/2013/738932
4. Puttaswamy and R. V. Jagadeesh, *Industrial & Engineering Chemistry Research*, **45**, 1563(2006), https://doi.org/10.1021/ie0509746
5. Yogeesha N. Nayak, S. L. Gaonkar, E. A. Musad Saleh and Ismail Hassan, *Journal of Saudi Chemical Society*, **26**, 101416(2022), https://doi.org/10.1016/j.jscs.2021.101416
6. T. Umemoto, S. Fukami, G. Tomizava, K. Harasava, K. Kavada and K. Tomita, *Journal of American Chemical Society*, **112**, 8563(2009), https://doi.org/10.1021/ja00179a047
7. K. M. Meenakshi and K. Vasanth Kumar Pai, *Journal of Chemistry*, **6**, 545(2009), https://doi.org/10.1155/2009/149032
8. P. T. Sowmya, K. M. Lokanath Rai, Anitha Sudhir and Sumana Y. Kotian, *Australian Journal of Chemistry*, **74**(10), 1089(2021), http://dx.doi.org/10.1071/CH21089
9. J. Ungula and H. C. Swart, *Journal of Alloys and Compounds*, **821**, 153459(2015), https://doi.org/10.1016/j.jallcom.2019.153459
10. H.S. Sonakshi, M.K. Arpitha, K.M. Vidyashree, H. P. Jayadevappa, *Asian Journal of Chemistry*, **37**, 313(2025), https://doi.org10.14233/ajchem.2025.32510

11. Ahmed Faried Abdel Hakiem, Ahmed Mohsen Kamal, Ahmed Safwat Aboraia, Refaat M Mahfouz, Ahmed A.K. Mohammed, Ibrahim A. Naguib, Mohammed E. Draz, *Microchemical Journal*, **206**, 111423 (2024), https://doi.org/10.1016/j.microc.2024.111423
12. Shimon Takahashi, Kenshi Takechi, Natsumi Jozukuri, Takahiro Niimura, Masayuki Chuma, Mitsuhiro Goda, Yoshito Zamami, Yuki IzawaIshizawa , Masaki Imanishi, Yuya Horinouchi, Yasumasa Ikeda, Koichiro Tsuchiya, Hiroaki Yanagawa, Keisuke Ishizawa, *European Journal of Pharmacology*, **902**, 174099(2021), https://doi.org/10.1016/j.ejphar.2021.174099
13. Jamelah S. Al-Otaibi, Y. Sheena Mary, Renjith Thomas, Savas Kaya, *Polycyclic Aromatic Compounds*, **42**, 1260(2022), https://doi.org/10.1080/10406638.2020.1773876
14. Guohong Xie, Xin Chang, Bal Ram Adhikari, Sapanbir S. Thind, Aicheng Chen, *Chinese Journal of Catalysis*, **37**, 1062(2016), https://doi.org/10.1016/S1872-2067(15)61101-9Get rights and content
15. Vinit B. Mahajan, Edwin M. Stone, *American Journal of Ophthalmology*,**150**,511(2010) https://doi.org/10.1016/j.ajo.2010.05.024
16. Manish Yadav, Vivek Upadhyay, Puran Singhal, Sailendra Goswami, Pranav S. Shrivastav, *Journal of Chromatography B*, **877**, 680(2009), https://doi.org/10.1016/j.jchromb.2009.01.042
17. Ayesha shaik, Varun Tandon, Ayesha Azmeen, *Chest Journal*, **156**, A2050(2019), https://doi.org/10.1016/j.chest.2019.08.2006
18. Gamal A. Saleh, Hassan F. Askal, Ibrahim H. Refaat, Ahmed H. Naggar, Fatma A.M. Abdel-aal, *Arabian Journal of Chemistry*, **9**, 143(2016), https://doi.org/10.1016/j.arabjc.2015.08.015
19. Debasis Mondal, *xPharm: The Comprehensive Pharmacology*, **87**,1(2007), https://doi.org/10.1016/B978-008055232-3.62841-7
20. WilliamW. Andrew, Debora, F Kimberlin Richard Whitley, BA Suzanne Cliver, S Patrick, MD Ramsey, *American Journal of Obstetrics and Gynecology*, **194**, 774(2006), https://doi.org/10.1016/j.ajog.2005.11.051
21. R. Anselmann, *Journal of Nanoparticle Research*, **3**, 329(2001), https://doi.org/10.1023/A:1017529712314
22. F. Feigl and V. Anger, Spot Test in Organic Analysis, Amsterdam, Edition. **7**, 376(2005); https://doi.org/10.1016/C2009-0-07233-X
23. J.C. Morris, J.A. Salazar and M.A. Wineman, *Journal of American Chemical Society*, **70**, 2036(1948), https://doi.org/10.1021/ja01186a016
24. E. Bishop and V.J. Jennings, *Talanta*, **1**, 197 (1958), https://doi.org/10.1016/0039-9140(58)80034-X
25. F.F. Hardy and J.P. Johnston, *Journal of Chemical Society*, **2**, 742(1973), https://doi.org/10.1039/p29730000742
26. B.G. Pryde and F.G. Soper, *Journal of Chemical Society*, 1514(1931), https://doi.org/10.1039/JR9310001514
27. A. Sukhdev and P. Puttaswamy, *Journal of Springer Plus*, **2**, 30(2013), https://doi.org/10.1186/2193-1801-2-30
28. D.K. Wolgemuth, S.D. Elmore, J.D. Cope, P.E. Sheridan, S.L. Stokes and J.P. Emerson, *Catalysis Communication*, **150**, 106275(2021), https://doi.org/10.1016/j.catcom.2020.106275
29. E.S. Amis, Solvent Effects on Reaction Rates and Mechanism, Academic Press: New York, 1672 (2007).
30. K.J. Laidler, Chemical Kinetics, Tata McGraw-Hill, New Delhi, Edition. 3, p. 544 (2003).

[RJC-9313/2025]